Supporting Information

Indium-Tin-Oxide Branched Nanowire and Poly(3-hexylthiophene) Hybrid Structure for Photorechargeable Supercapacitor

Wan Jae Dong,* Won Seok Cho, Jong-Lam Lee*

Department of Materials Science and Engineering, Pohang University of Science and Technology (POSTECH), Pohang 790-784 (Korea)
E-mail: jllee@postech.ac.kr, wjdong@postech.ac.kr

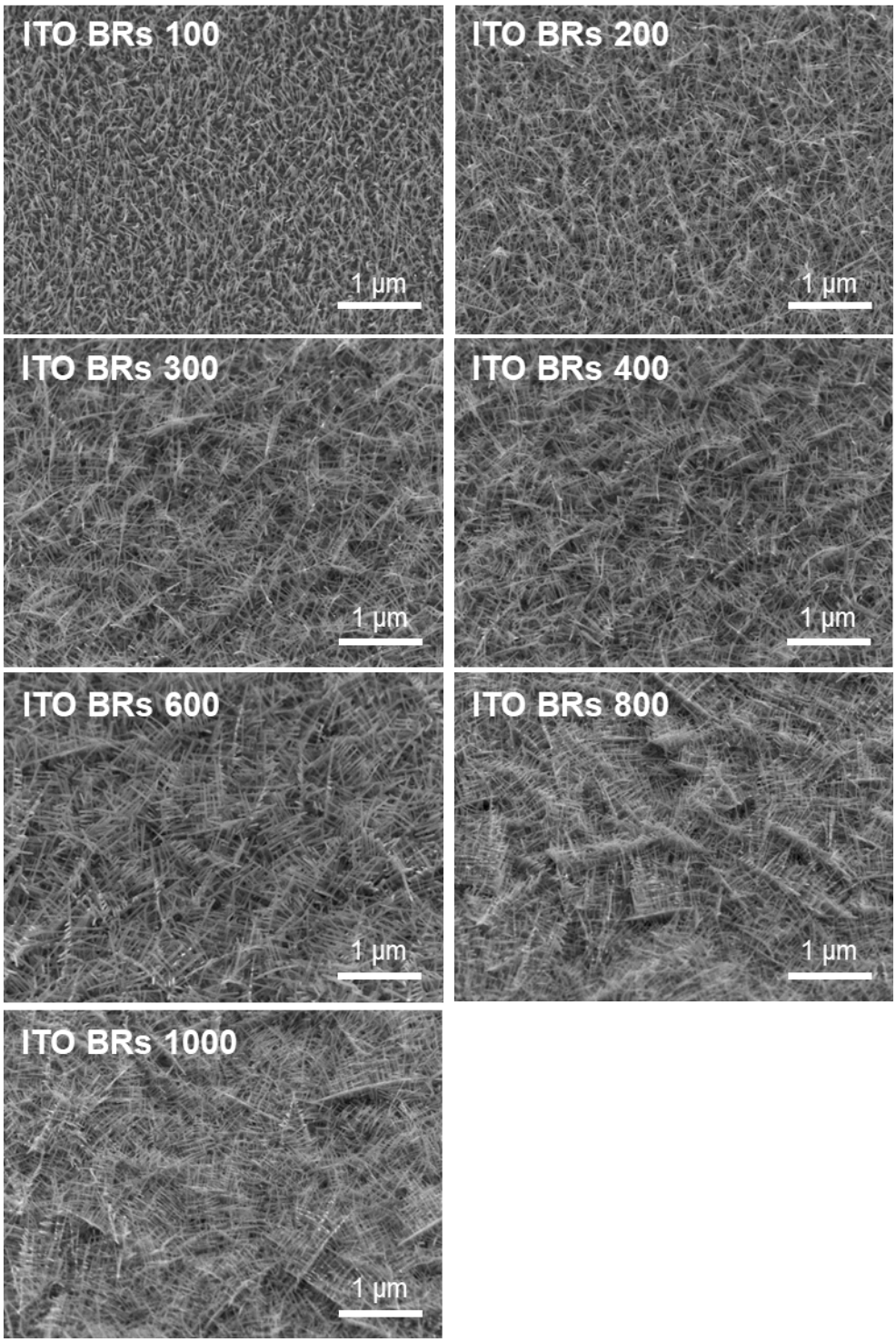

Figure S1. 45º-tilt view SEM images of ITO BRs. The length of ITO BRs gradually increases and they entangle each other as the thicknesses of ITO BRs increase from 100 to 1000 nm.

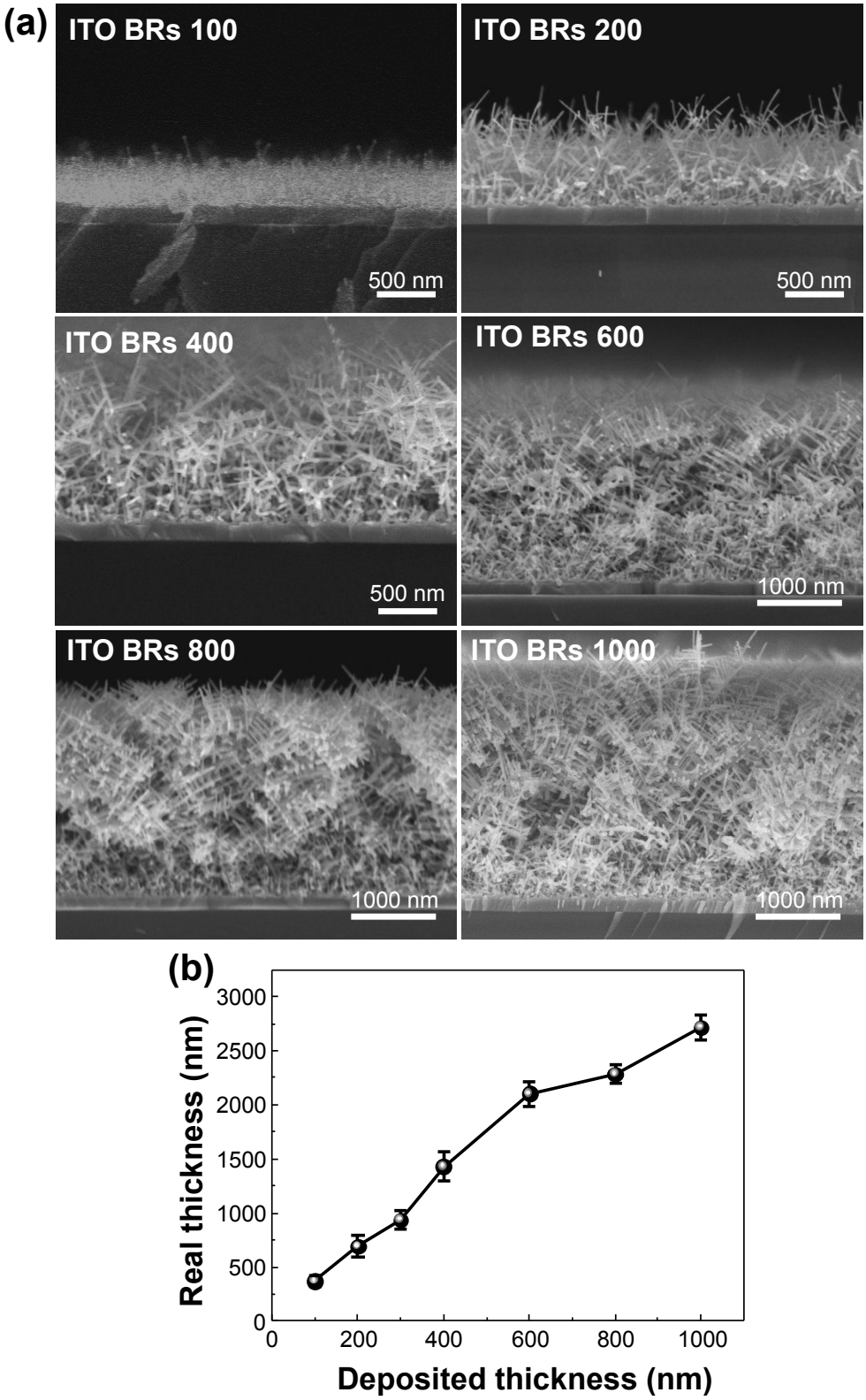

Figure S2. (a) Cross-sectional SEM images of ITO BRs. (b) Measured real thickness of ITO BRs plotted as a function of deposited thickness from 100 to 1000 nm.

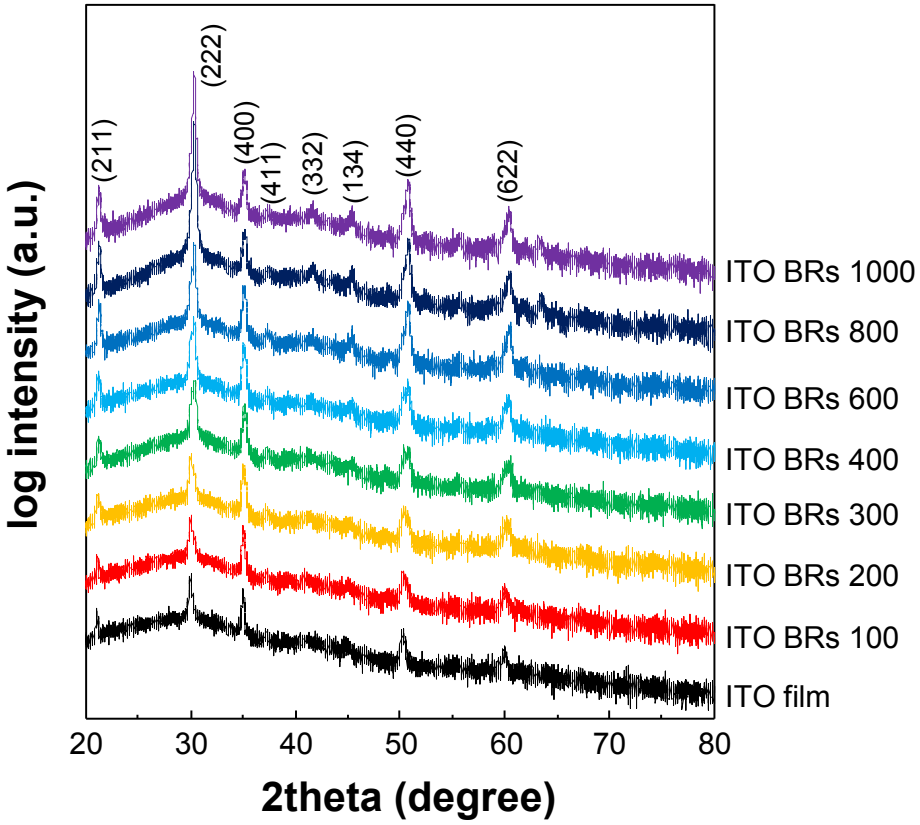

Figure S3. X-ray diffraction patterns of ITO BRs. ITO film showed polycrystalline characteristics with (222), (400), (440), (622), (211), and (134) planes. Although ITO BRs have a single crystal structure with {100} family planes, the diffraction peaks from other planes could be detected due to the underlying ITO film.

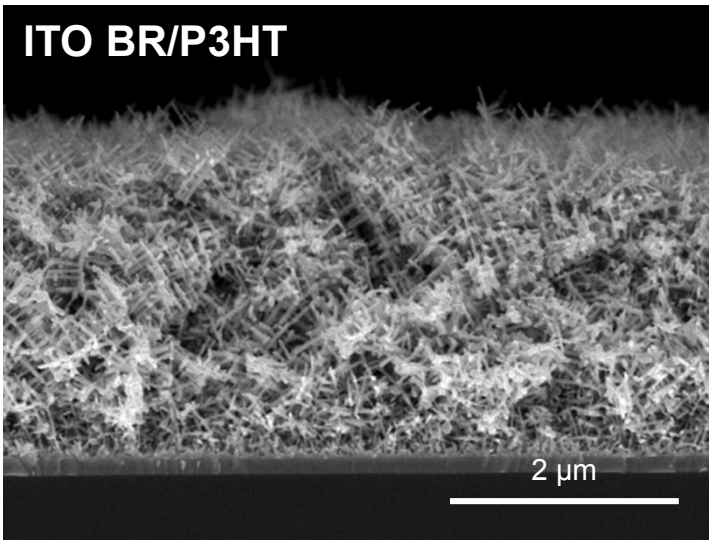

Figure S4. Cross-sectional SEM image of ITO BR 1000/P3HT

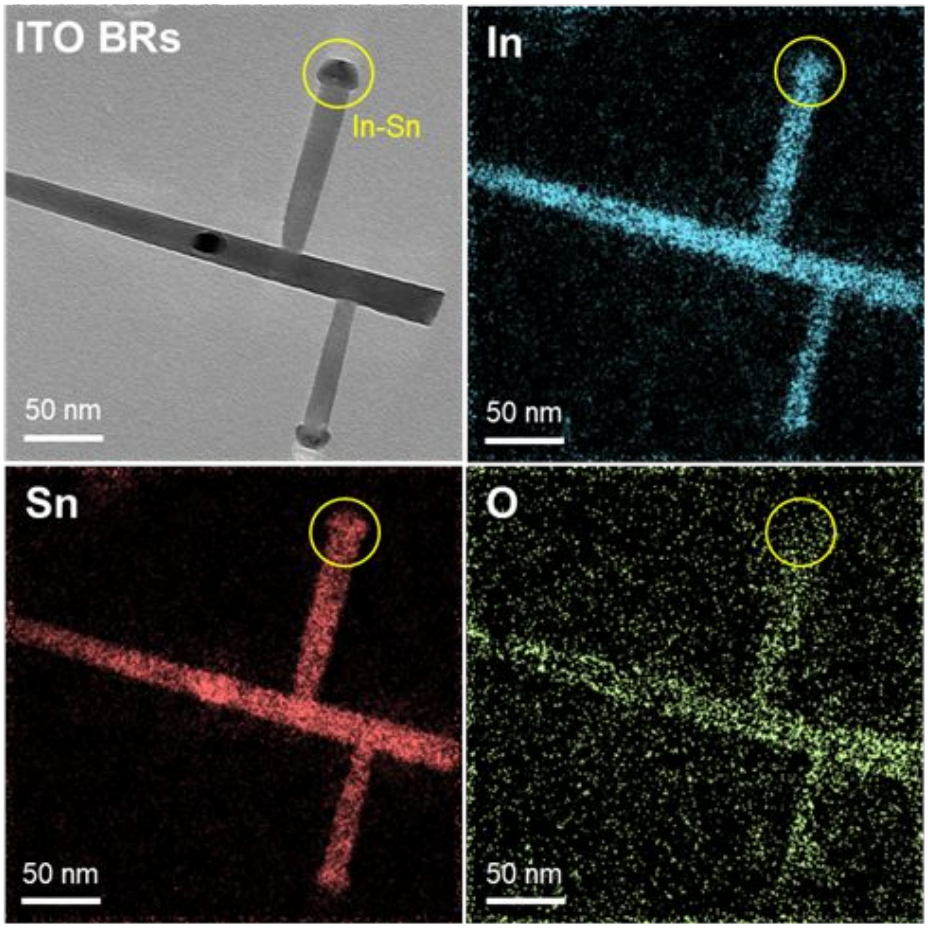

Figure S5. TEM-EELS elemental maps of ITO BRs and (blue: indium; red: tin; green: oxygen).

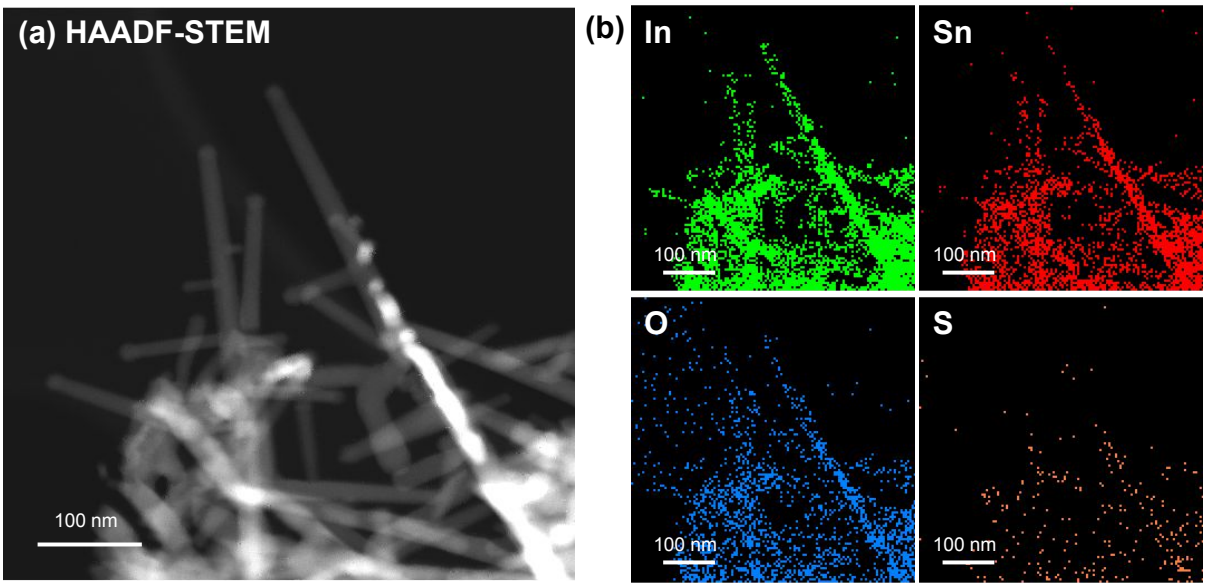

Figure S6. (a) High-angle annular dark-field scanning transmission electron microscopy (HAADF-STEM) image of ITO BR/P3HT structure. (b) Energy-dispersive X-ray spectroscopy (EDS) elemental maps of indium (green), tin (red), oxygen (blue), and sulfur (orange).

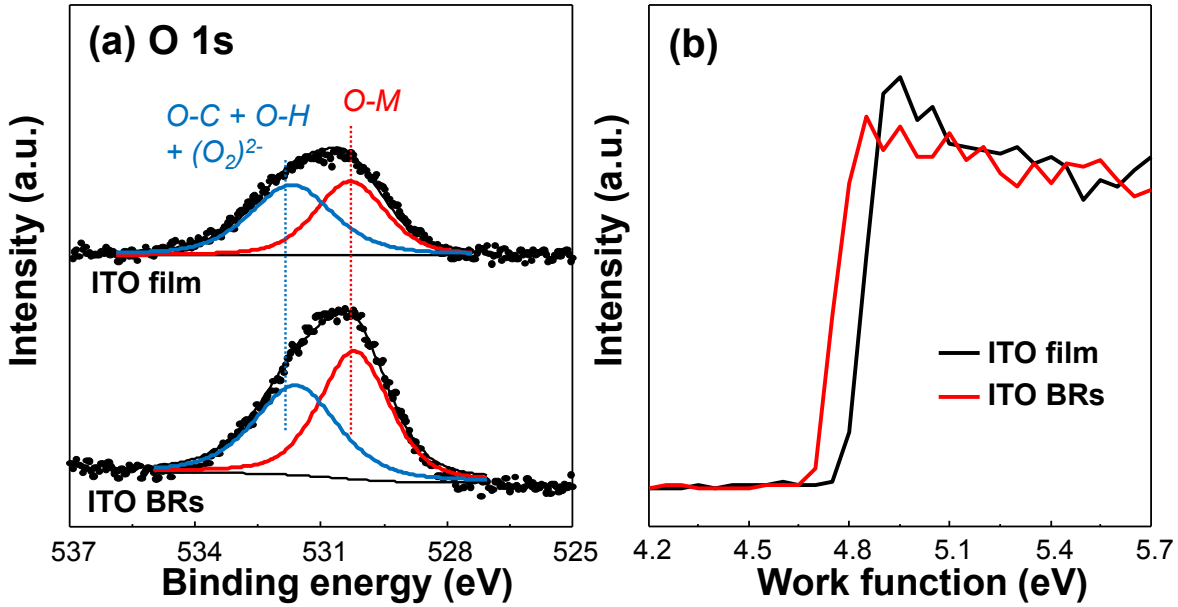

Figure S7. (a) O 1s XPS spectra, and (b) work function of ITO film and ITO BRs.

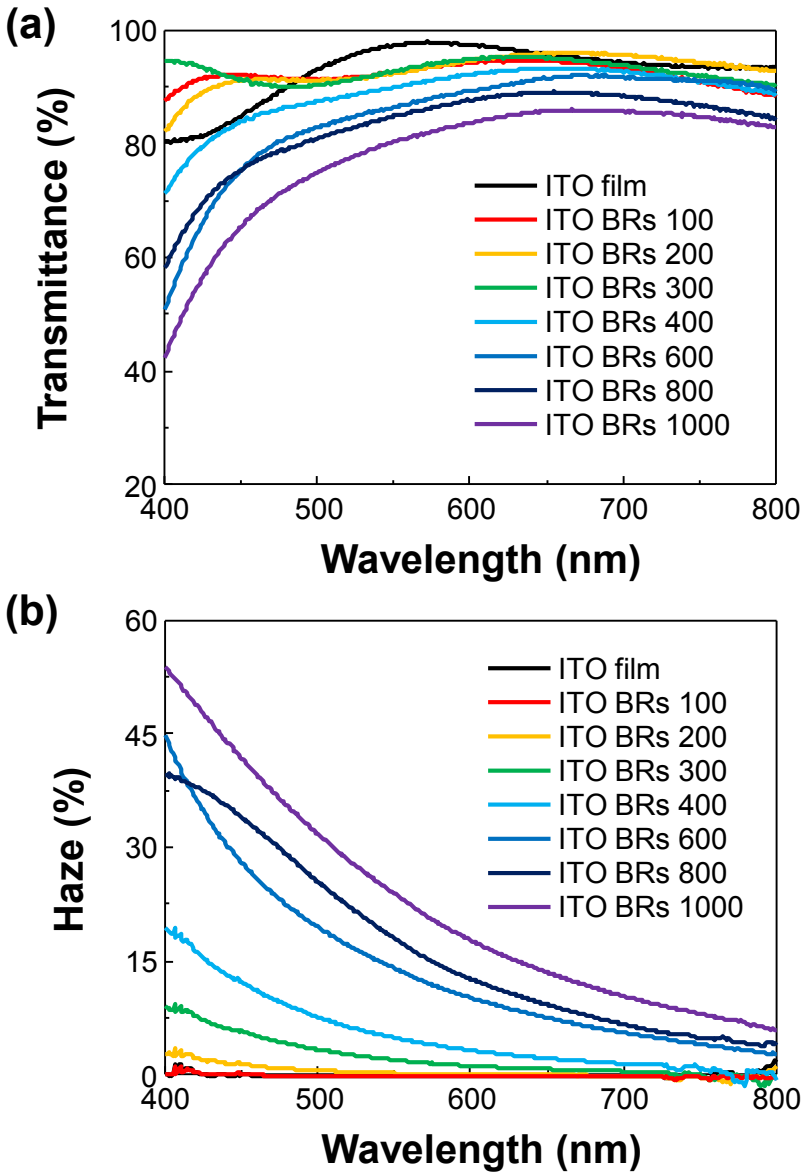

Figure S8. (a) Optical transmittance and (b) haze of ITO BRs measured at visible wavelength (λ = 400 ~ 800 nm). Haze was calculated by dividing the diffused transmittance by the total transmittance.

Electrochemical Properties of ITO BRs

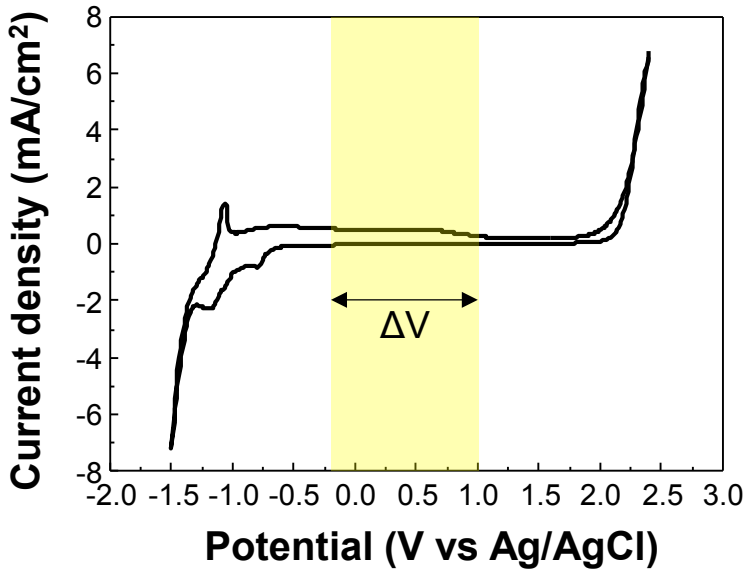

Figure S9. Cyclic voltammetry (CV) curves of ITO BRs electrode at a scan rate of 100 mV/s. The electrical double-layer capacitor was evaluated in a potential window of -0.2 to 0.8 $V_{Ag/AgCl}$ where no oxidation or reduction reaction occurred.

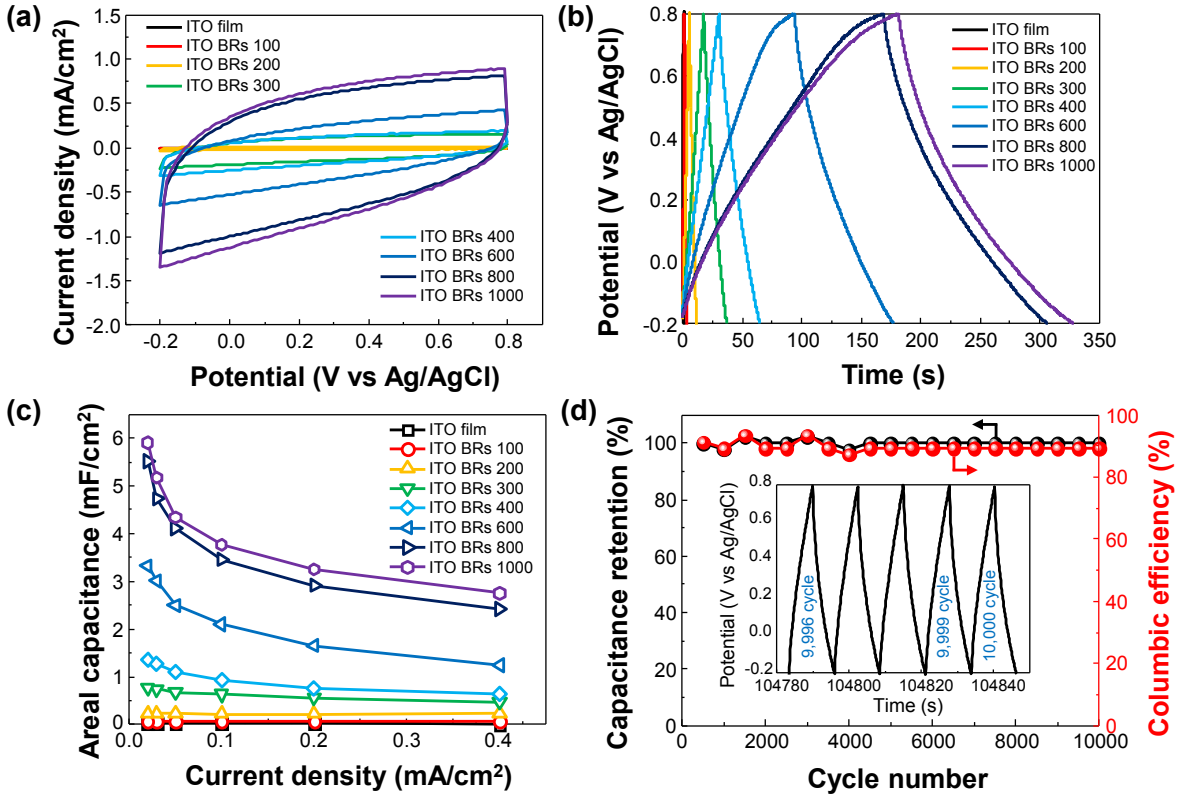

Figure S10. Electrochemical measurement of ITO BRs in a three-electrode configuration in 1 M Na_2SO_4 electrolyte. (a) CV curves of ITO BRs with different thicknesses at a scan rate of 1000 mV/s. (b) GCD curves of ITO BRs with different thicknesses at a current density of 20 μA/cm^2. (c) Areal capacitance as a function of current density determined from the GCD curves. (d) Cyclic stability of ITO BRs 1000 at current density of 0.2 mA/cm^2, showing capacitance retention > 93% and columbic efficiency > 87% after 10,000 cycles.

The cyclic voltammetry (CV) curves of ITO BRs were measured at different scan rates (Figure S11) and the CV curves at a scan rate of 1000 mV/s were compared to show the effect of t_{ITO} on electrochemical properties (Figure S10a). The CV curves of ITO BRs exhibited a quasi-rectangular shape and absence of redox peaks, demonstrating excellent double-layer capacitive charge storage characteristics. The increase in capacitance with t_{ITO} was obvious as ITO BRs became denser and larger. The Nyquist plots, measured by electrochemical impedance spectroscopy (EIS) in the frequency range from 0.1 to 1 mHz at open-circuit potential, denote the nearly vertical straight line at the low-frequency regions,

illustrating an ideal capacitive behavior of the ITO BRs (Figure S12). The galvanostatic charge/discharge (GCD) measurement was performed at a potential window of -0.2 ~ 0.8 $V_{Ag/AgCl}$ with varying current densities ranging from 0.02 to 0.4 mA/cm^2 (Figure S13) and the GCD curves at a current density of 0.02 mA/cm^2 were compared (Figure S10b). The GCD curves showed nearly triangular shapes, confirming the double layer capacitive behavior and reversible faradaic reactions between Na^+ ions in the electrolyte and ITO BRs. The obtained C_{areal} values from GCD curves of ITO BRs increase with t_{ITO} due to the increased active surface area (Figure S10c). The C_{areal} of the ITO BRs 1000 was found to be 5.90 mF/cm^2 at a current density of 0.02 mA/cm^2, which decreased to 2.75 mF/cm^2 when the current density was increased to 0.4 mA/cm^2.

The cycling stability of a representative electrode (ITO BRs 1000) was tested over 10,000 GCD cycles at a current density of 0.2 mA/cm^2. The capacitance retention (93% over 10,000 cycles) evidences the excellent charge/discharge stability of ITO BRs (Figure S10d). Moreover, the columbic efficiency, the ratio between τ_d and τ_c (charging time), was higher than 87% after 10,000 cycles. The good cycling stability of ITO BRs might be attributed to the highly porous and network structure. The porous structure provides a large surface area and enables the quick passage of electrolyte ions.

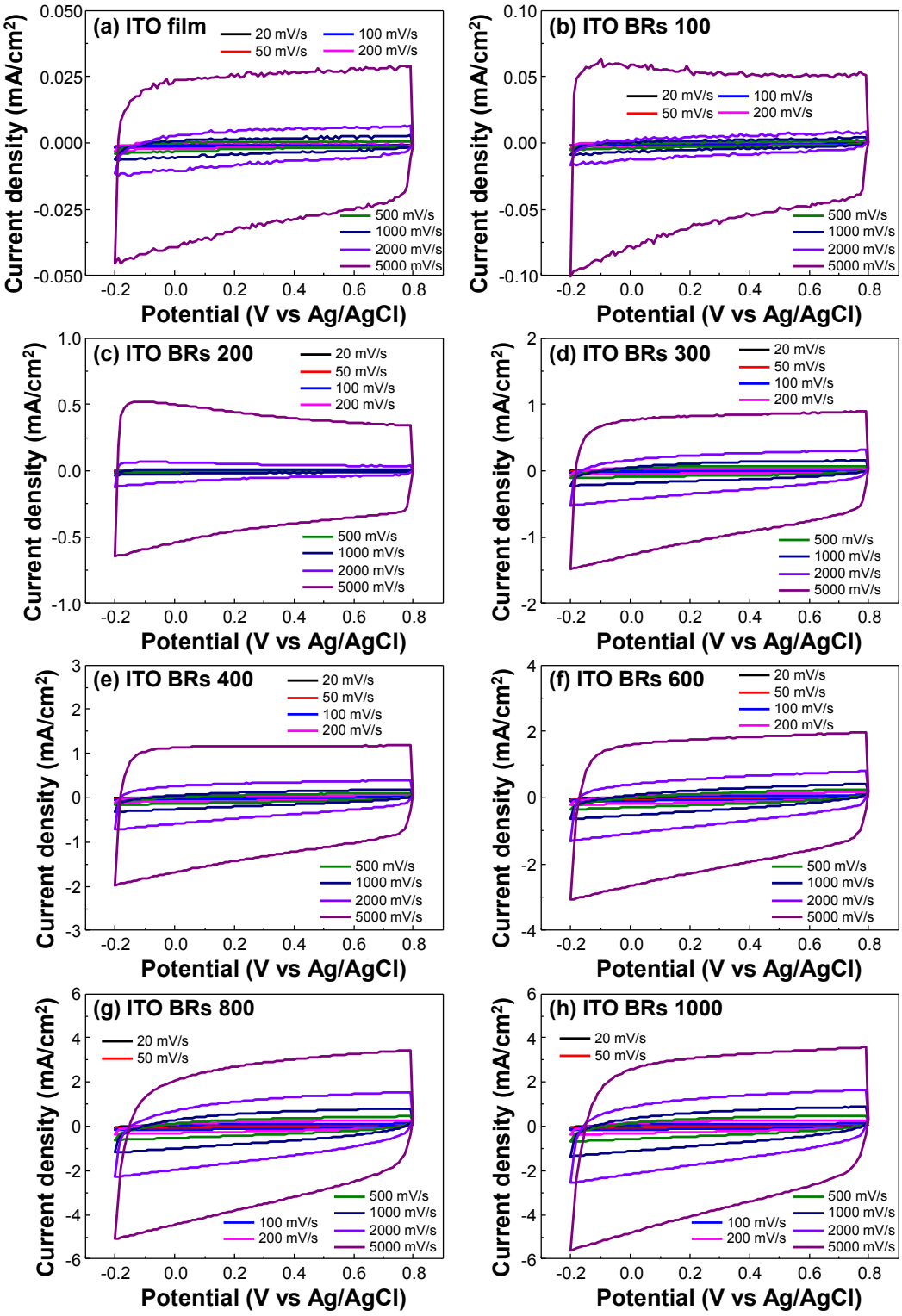

Figure S11. CV curves for the electrodes with (a) ITO film and ITO BRs thicknesses of (b) 100, (c) 200, (d) 300, (e) 400, (f) 600, (g) 800, (h) 1000 nm at different scan rates (20 ~ 5000 mV/s).

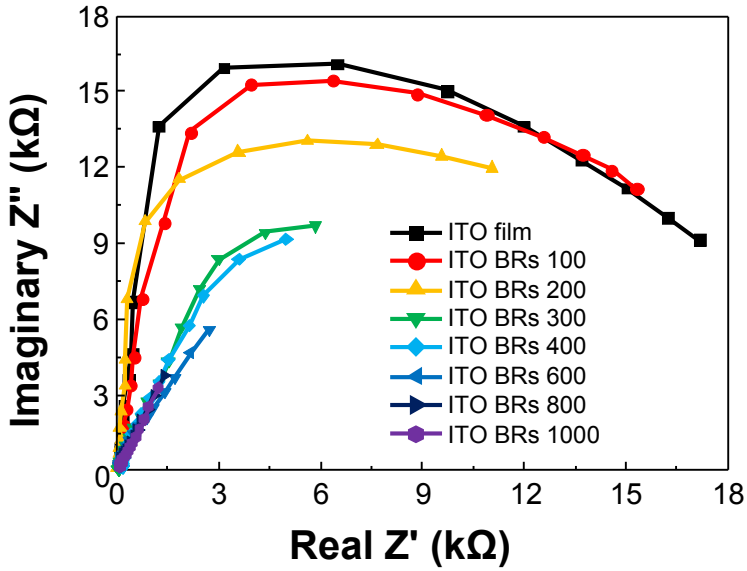

Figure S12. Nyquist impedance plots of ITO BRs at a frequency range of 1 MHz to 0.1 Hz at the open-circuit potential.

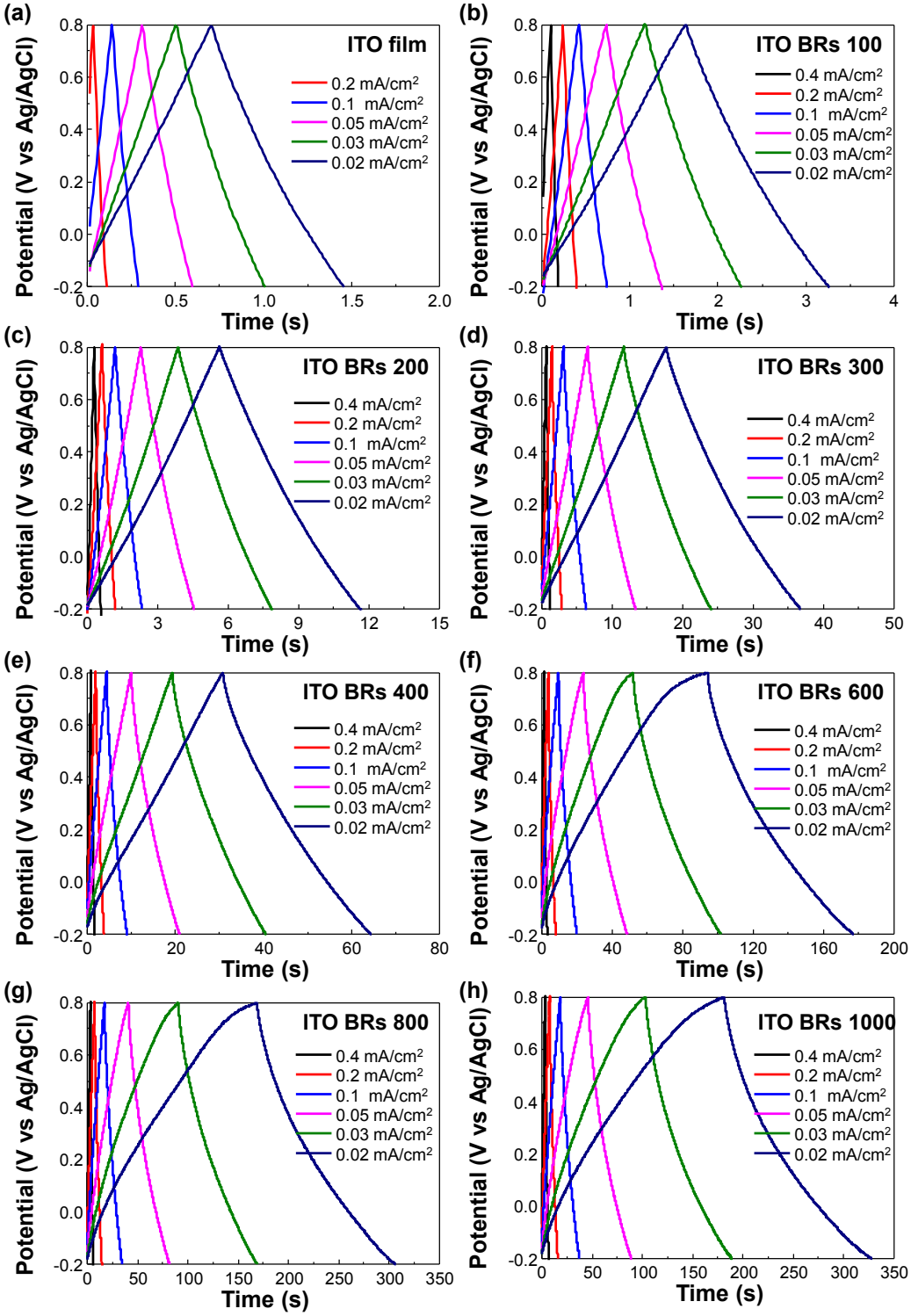

Figure S13. Galvanostatic charge/discharge (GCD) curves for the electrodes with (a) ITO film and ITO BRs thicknesses of (b) 100, (c) 200, (d) 300, (e) 400, (f) 600, (g) 800, (h) 1000 nm at different current densities (0.02 ~ 0.4 mA/cm^2).

Photoelectrochemical Properties of ITO BR/P3HT

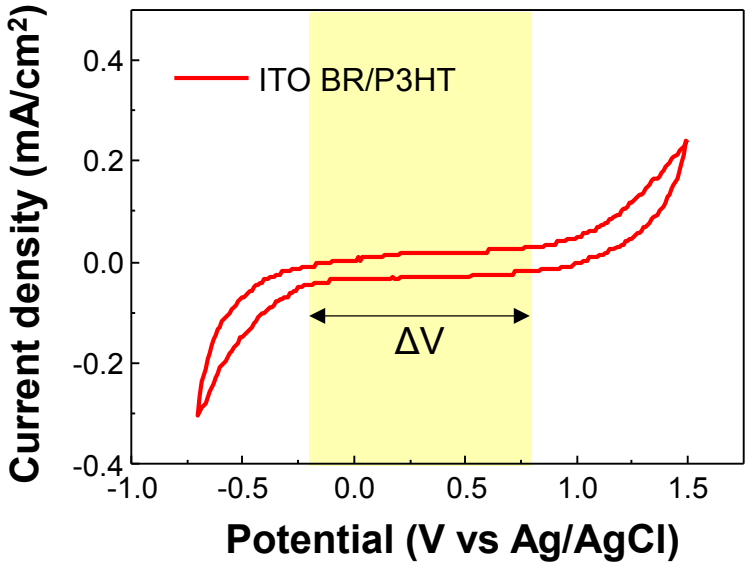

Figure S14. CV curves of ITO BR/P3HT electrode at a scan rate of 100 mV/s. The electrical double-layer capacitor was evaluated in a potential window of -0.2 to 0.8 $V_{Ag/AgCl}$ where no oxidation or reduction reaction occurred.

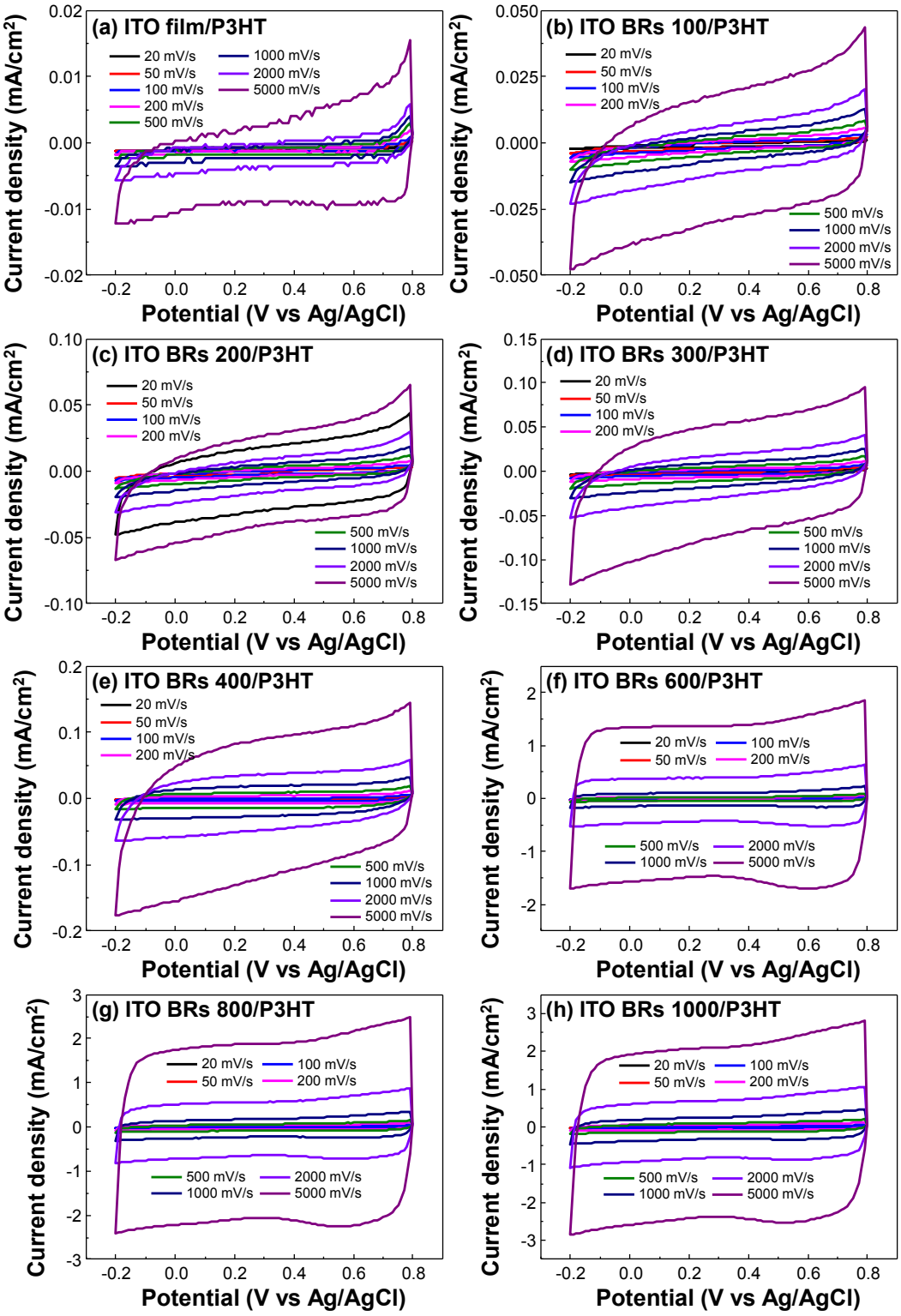

Figure S15. CV curves for (a) ITO film/P3HT and ITO BR/P3HT with ITO BRs thicknesses of (b) 100, (c) 200, (d) 300, (e) 400, (f) 600, (g) 800, (h) 1000 nm at different scan rates (20 ~ 5000 mV/s).

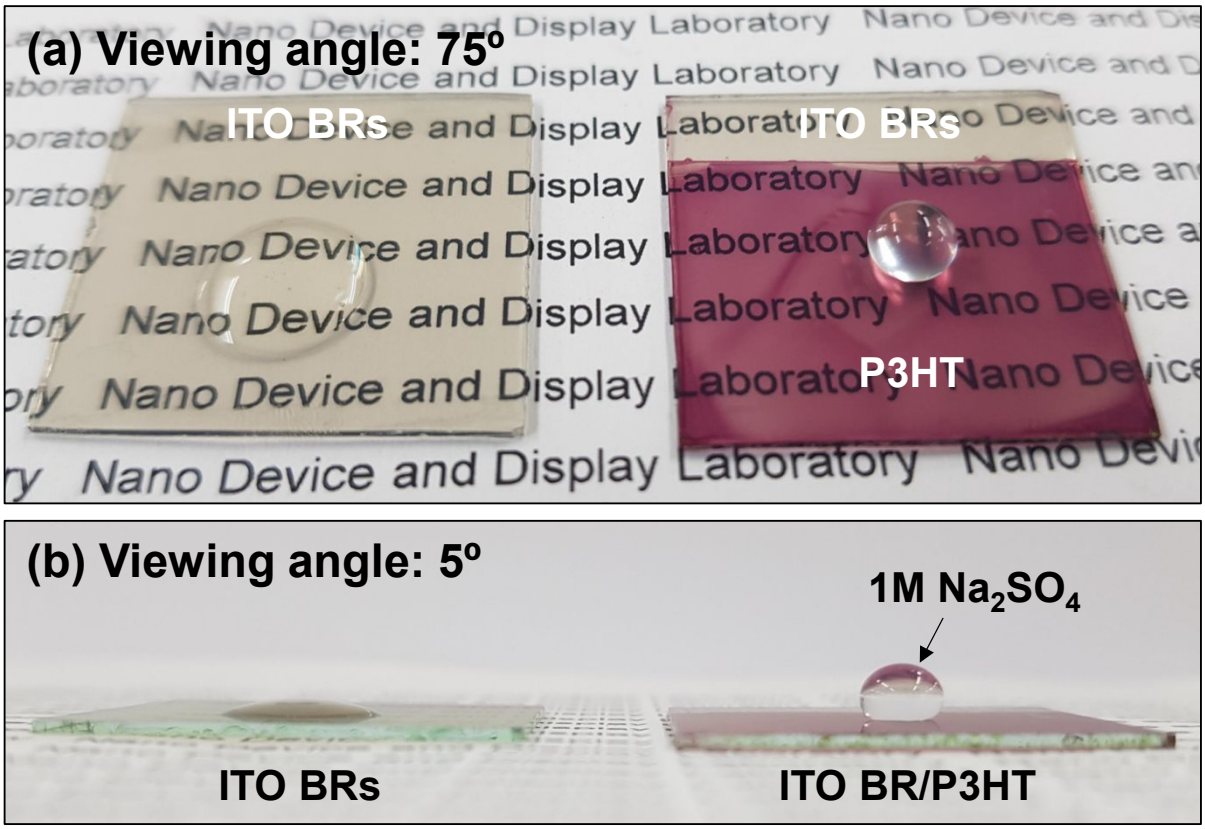

Figure S16. Photographs of water droplets (50 μL) on ITO BRs (left) and ITO BR/P3HT (right) at the viewing angle of (a) 75º and (b) 5º. The larger contact angle of the water droplet on ITO BR/P3HT than on ITO BRs proves that the surface has changed from hydrophilic to hydrophobic after coating P3HT.

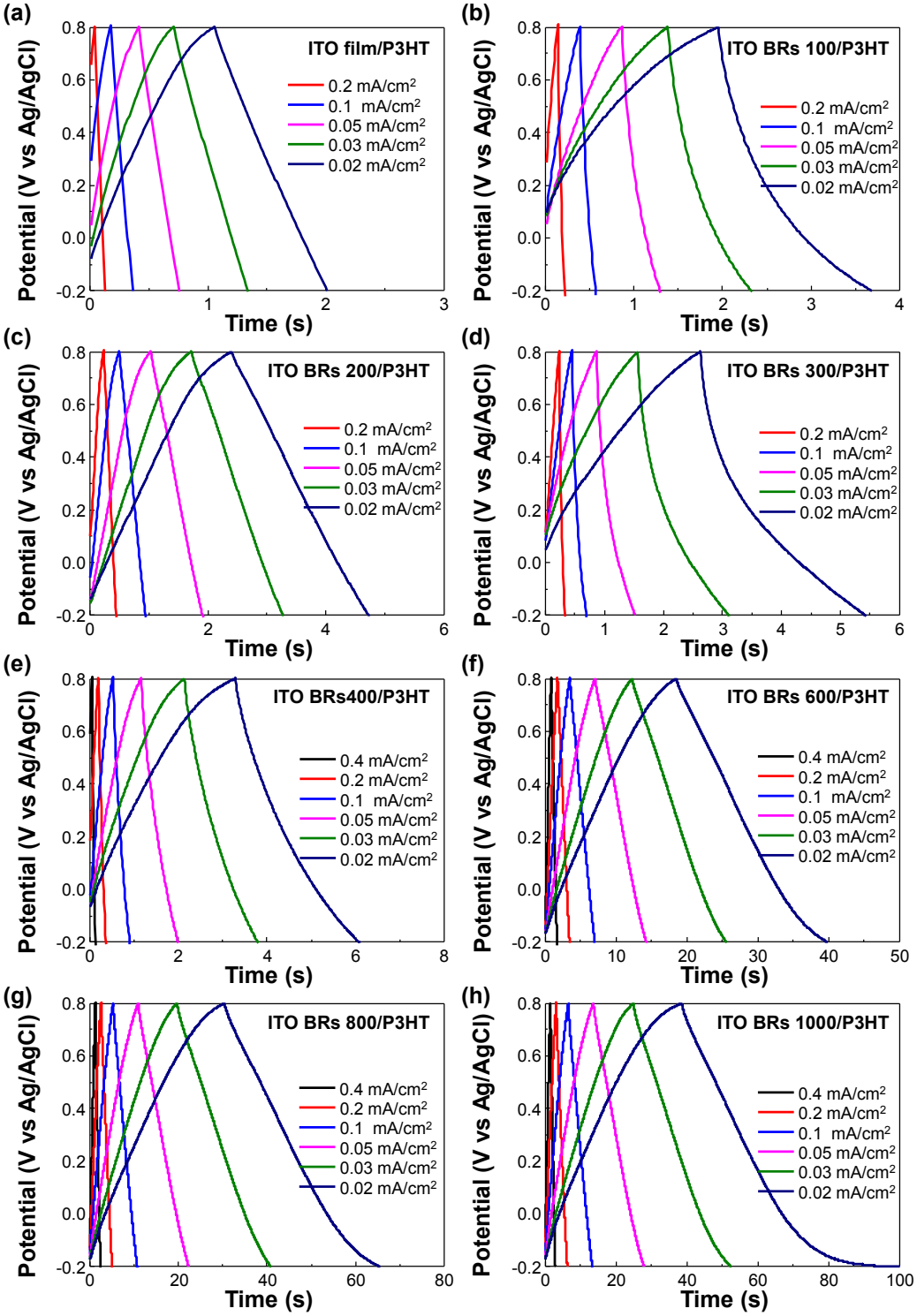

Figure S17. GCD curves for (a) ITO film/P3HT and ITO BR/P3HT with ITO BRs thicknesses of (b) 100, (c) 200, (d) 300, (e) 400, (f) 600, (g) 800, (h) 1000 nm at different current densities (0.02 ~ 0.4 mA/cm^2).

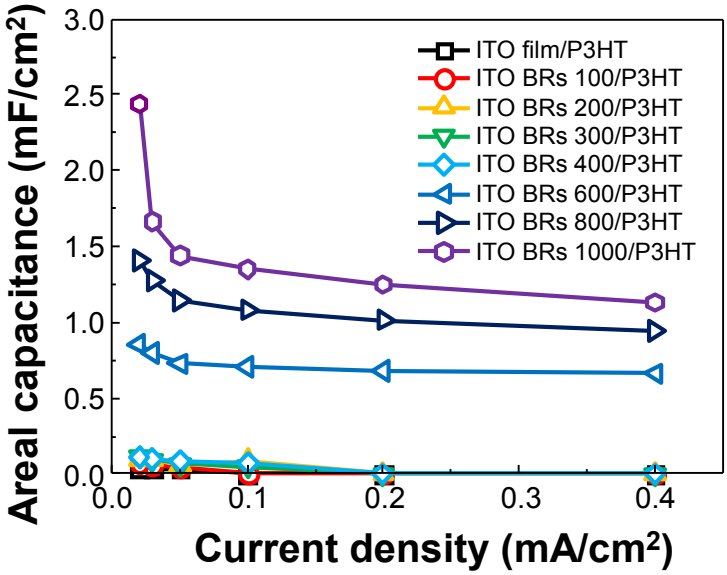

Figure S18. Electrochemically measured areal capacitance of ITO BR/P3HT electrode in a three-electrode configuration in 1 M Na_2SO_4 electrolyte.

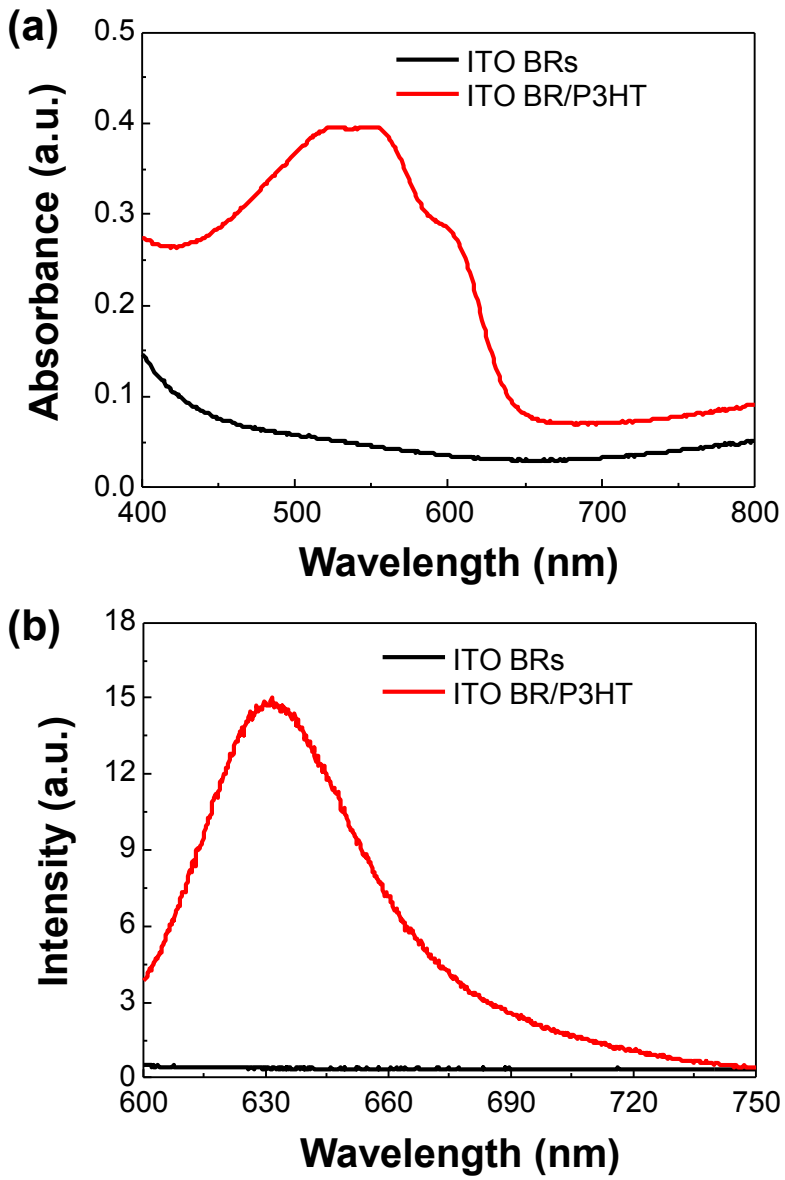

Figure S19. (a) Light absorbance spectra and (b) steady-state photoluminescence (PL) spectra of ITO BRs and ITO BR/P3HT. After P3HT coating on ITO BRs, light absorption was noticeable at a wavelength of 400 to 650 nm due to the bandgap of P3HT (~1.9 eV). PL spectra were obtained by an excitation wavelength of 530 nm.

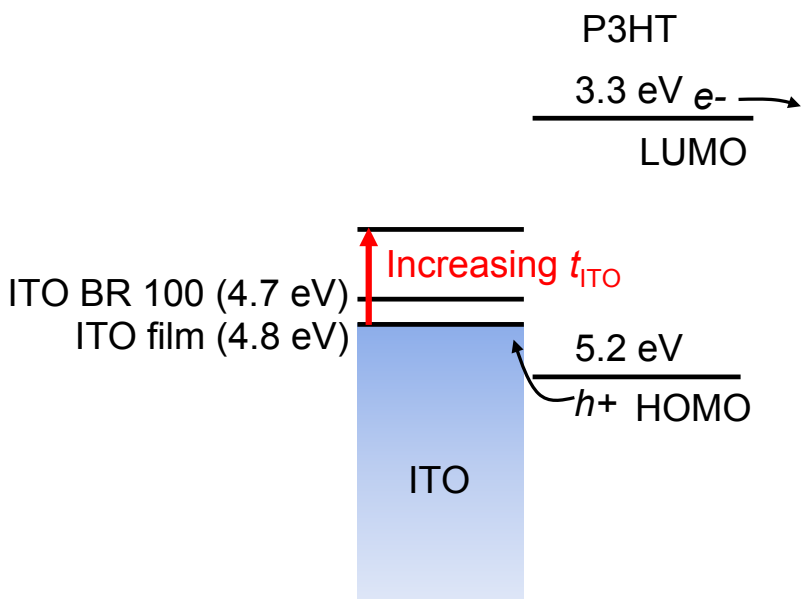

Figure S20. Schematic band diagram of ITO electrodes and P3HT. There is hole extraction barrier at ITO/P3HT interface. The charge transport barrier increases with t_{ITO} due to decreased WF of ITO BRs.

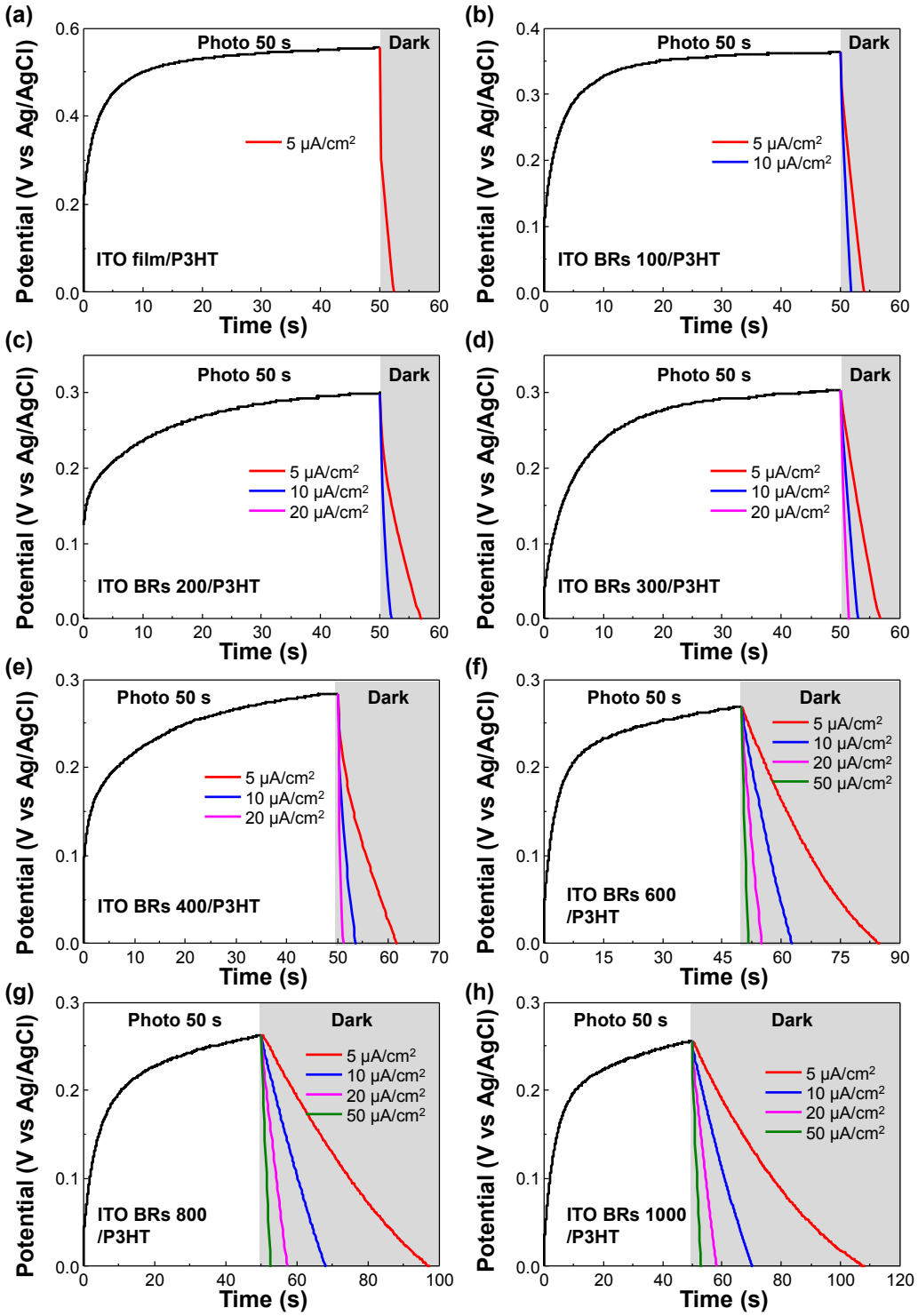

Figure S21. Photocharging and discharging curves for (a) ITO film/P3HT and ITO BR/P3HT with ITO BRs thicknesses of (b) 100, (c) 200, (d) 300, (e) 400, (f) 600, (g) 800, (h) 1000 nm. Photocharging was conducted for 50 s under light intensity of 100 mW/cm^2 and electrochemical discharging was done in the dark at different current densities (5 ~ 50 μA/cm^2).

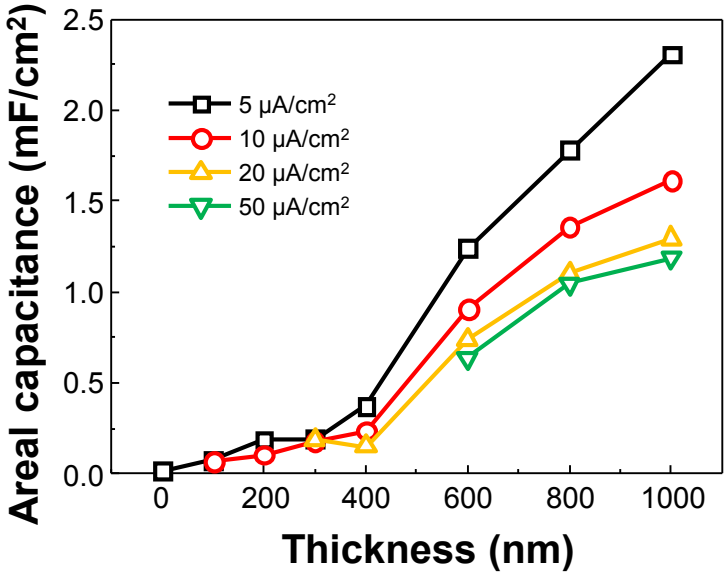

Figure S22. Areal capacitance of photocharged ITO BR/P3HT.

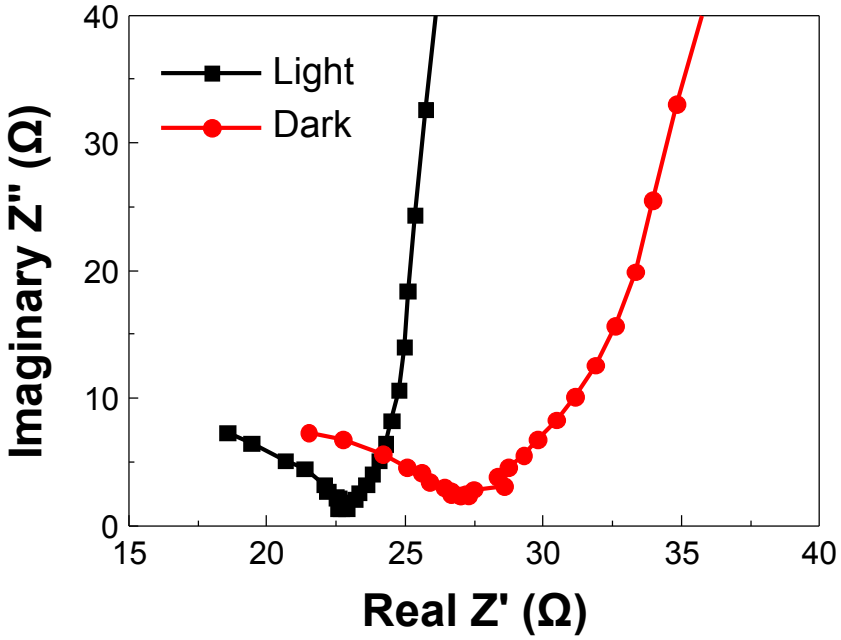

Figure S23. Nyquist impedance plots of ITO BR/P3HT at the open-circuit potential at 30 mV amplitude under light and dark conditions.

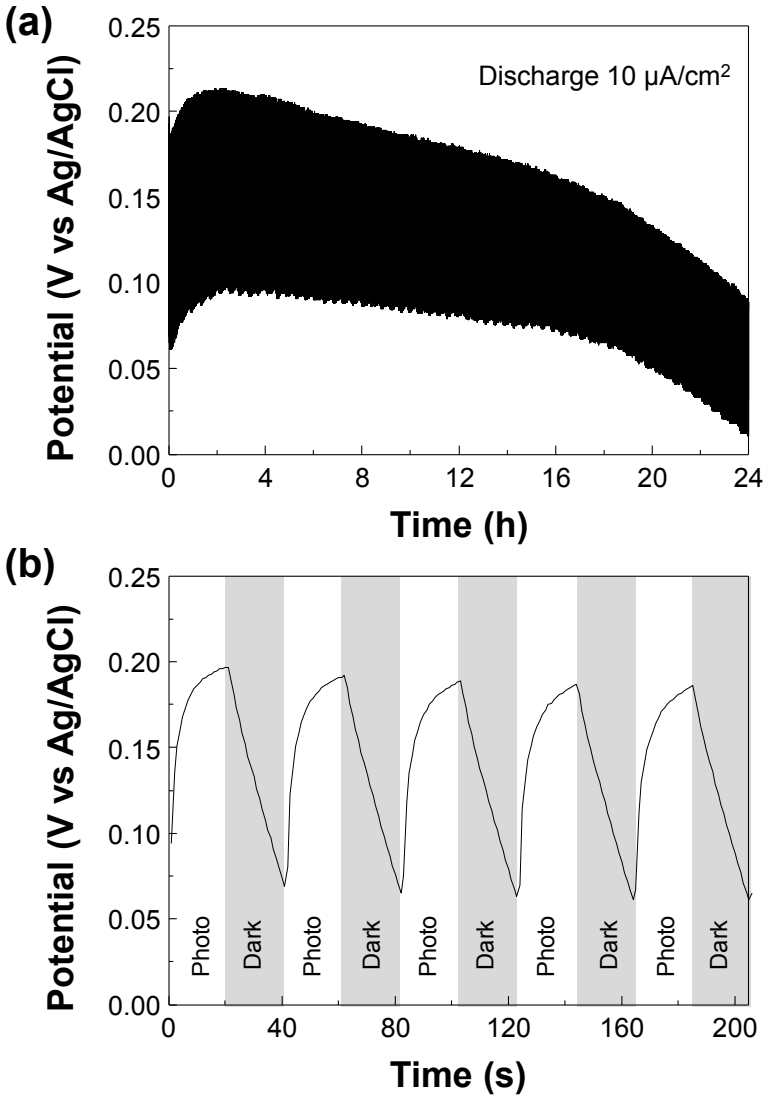

Figure S24. (a) Cyclic stability of ITO BR/P3HT at discharging current density of 10 μA/cm^2 under chopped light illumination. (b) Photo-charging/discharging curves for the initial 5 cycles.

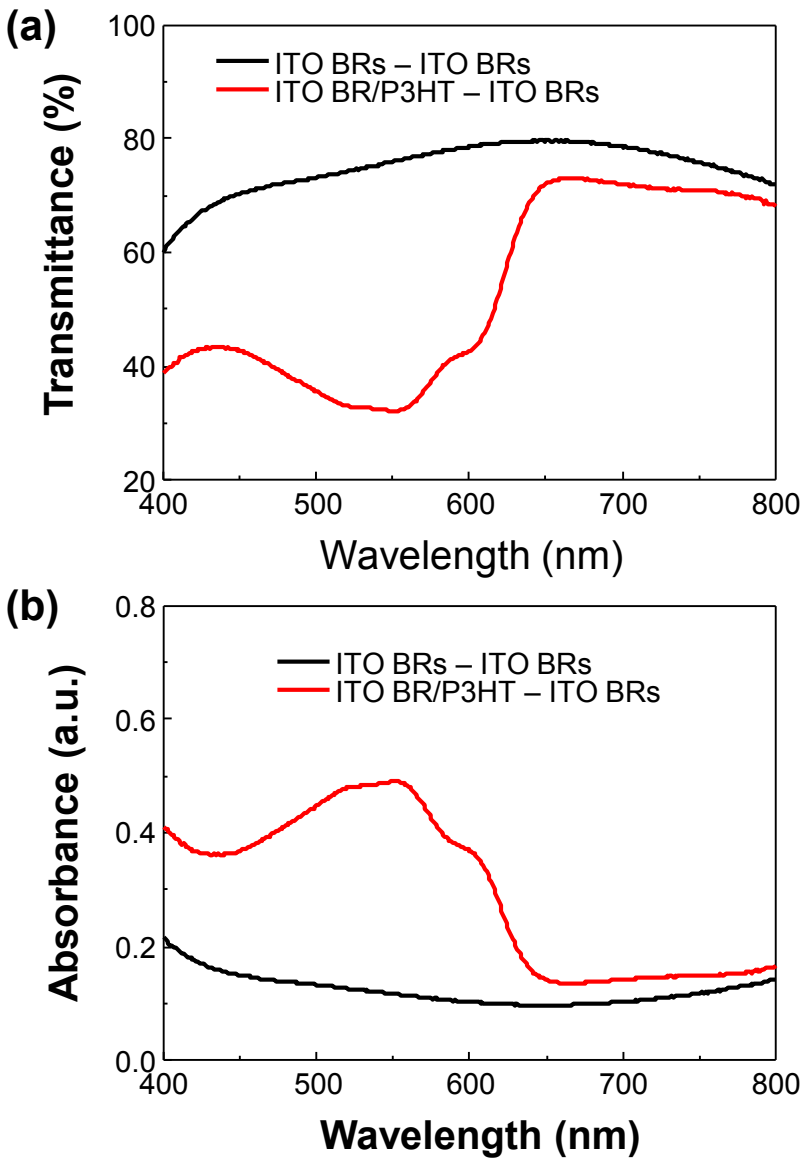

Figure S25. (a) Optical transmittance and (b) light absorbance spectra of photorechargeable energy storage devices of ITO BRs–ITO BRs (device 1) and ITO BR/P3HT–ITO BRs (device 2).

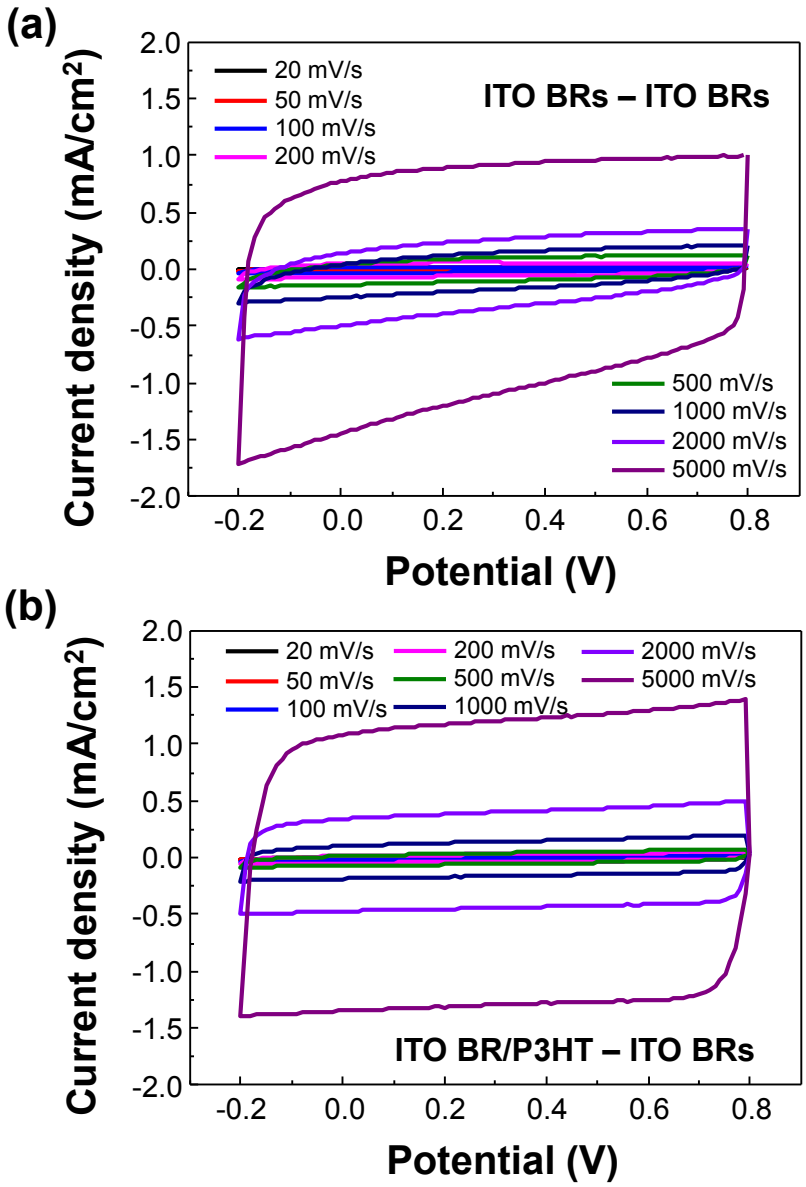

Figure S26. CV curves for the photorechargeable energy storage devices for (a) ITO BRs–ITO BRs (device 1) and (b) ITO BR/P3HT–ITO BRs (device 2).

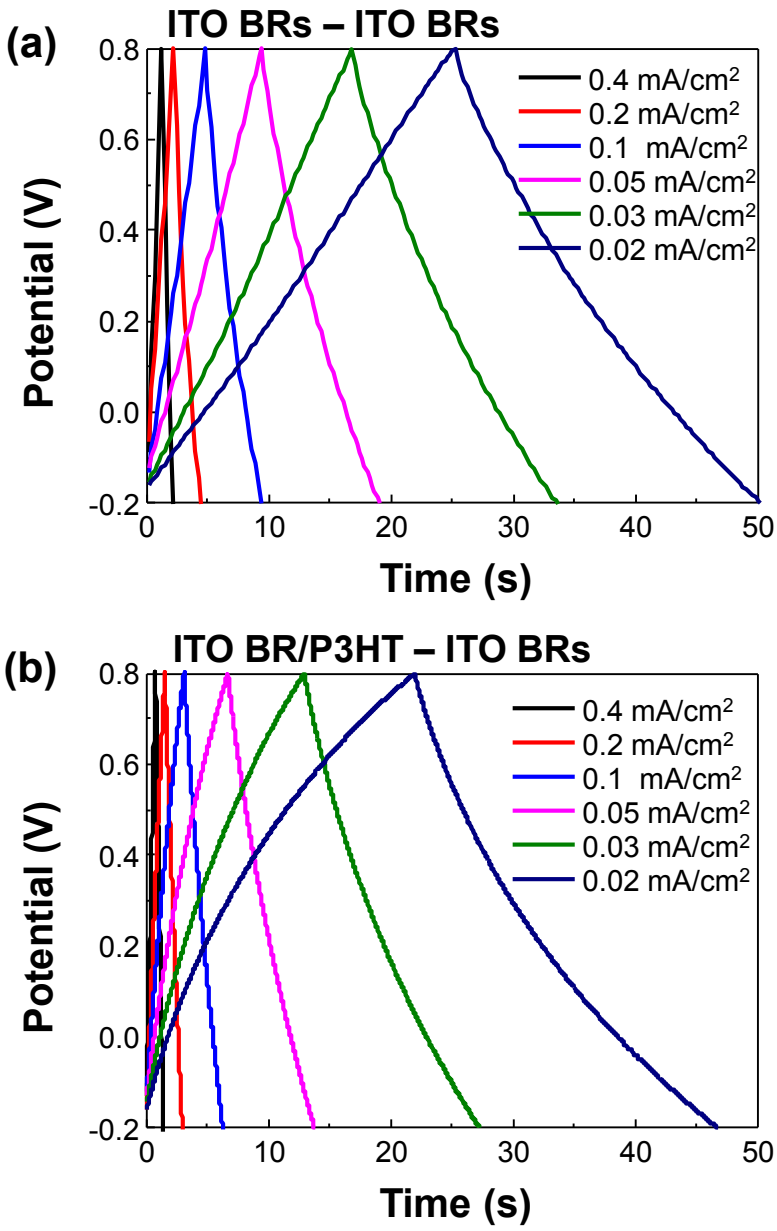

Figure S27. GCD curves for the photorechargeable energy storage devices for (a) ITO BRs–ITO BRs (device 1) and (b) ITO BR/P3HT–ITO BRs (device 2).

Calculation of photo-charging conversion efficiency

We calculated the photo-charging conversion efficiency of ITO BR/P3HT photorechargeable supercapacitor using the following equations;

$$\eta = \frac{E_{out}}{Ein} \times 100\% = \frac{E_a}{P_{in} \times t} \times 100\%$$

$$\eta = \frac{E_{out}}{Ein} \times 100\% = \frac{(0.024\ \ \mu Wh\ \ cm^{-2}) \times 3600(s)}{100\ \ (mWcm^{-2}) \times 50(s)} \times 100\%$$

$$\eta \approx 0.0017\%$$

where E_a is the energy density, P_{in} is the light intensity, and t is photo-charging time. The photo-charging conversion efficiency (η) was ~0.0017%.